500-MHz Proton NMR Evidence for Two Solution Structures of the Common Arm Base-Paired Segment of Wheat Germ 5S Ribosomal RNA†

Jiejun Wu‡ and Alan G. Marshall*,‡,§

Department of Biochemistry, 484 West 12th Avenue, and Department of Chemistry, 120 West 18th Avenue, The Ohio State University, Columbus, Ohio 43210

Received July 31, 1989

ABSTRACT: The base-pair protons of the common arm duplex fragment of wheat germ (*Triticum aestivum*) ribosomal 5S RNA have been identified and assigned by means of 500-MHz proton NMR spectroscopy. The two previously reported extra base pairs within the fragment [Li et al. (1987) *Biochemistry 26*, 1578–1585] are now explained by the presence of two distinct solution structures of the common arm fragment (and its corresponding base-paired segment in intact 5S rRNA). The present conclusions are supported by one- and two-dimensional proton homonuclear Overhauser enhancements in H_2O and by temperature variation and Mg^{2+} titration of the downfield ^1H NMR spectrum. The difference between the two conformers is most likely due to difference in helical tightness. Some additional amino proton resonances have also been assigned.

5S rRNA is the next largest RNA to tRNA, and its higher order structure has been under study for many years. A four-stem "universal" model for both prokaryotic and eukaryotic 5S rRNA secondary structures (Delihas & Andersen, 1982; 1984), based on an extension of previously proposed minimal structures (Nishikawa & Takemura, 1974; Fox & Woese, 1975; Luehrsen & Fox, 1981), has gained general acceptance. Much of the strongest supporting evidence has come from proton nuclear magnetic resonance (^1H NMR), specifically, proton homonuclear nuclear Overhauser enhancement (NOE). The NOE method can be used to identify base-pair type (A·U, G·C, G·U) as well as base-pair sequence (Johnston & Redfield, 1978, 1981; Sanchez et al., 1980; Hare & Reid, 1982a,b; Roy et al., 1982; Chang & Marshall, 1986). As noted in a recent comprehensive review of 5S rRNA NMR experiments (Marshall & Wu, 1990), the NOE experiment works best when performed on enzyme-cleaved 5S rRNA fragments rather than on intact 5S rRNA molecules.

The secondary structure of wheat germ (*Triticum aestivum*) 5S rRNA has been extensively characterized by ^1H NMR (Li & Marshall, 1985, 1986; Li et al., 1987). Specifically, a fragment of 5S rRNA (residues 26–51) produced by ribonuclease T1 cleavage contains helix III in the standard model and is also called the *common arm* fragment (see Figure 1A,B). (We shall refer to it as the *B2 fragment* from here on.) Several additional resonances (beyond those predicted by the standard model) were detected in the "downfield" ^1H NMR chemical shift region (9–15 ppm) in which base-paired protons are characteristically found. Two of the additional resonances could be explained by adding two base pairs (G_{41}·C_{34} and A_{42}·U_{33}) to the Luehrsen–Fox model (Figure 1C). Because the two proposed new base pairs involved the highly conserved GAAC segment of 5S rRNA, that peak assignment offered an explanation for the lack of binding between the 5S rRNA GAAC segment and the similarly conserved GTψC segment of tRNAs (Li et al., 1987).

In this paper, we present new evidence which shows that the observed extra proton resonances in the B2 fragment arise not from new intraloop base pairs but rather from *two NMR-distinguishable solution conformations* of the same 5S rRNA molecule. The "additional" resonances may now be assigned to base-paired imino protons and unpaired slow-exchanging imino protons in the loop region, for *each of the two conformers*. Each conformer has features consistent with the Luehrsen–Fox model, with a tight structure in the loop–helix junction and base-stacking extending into the hairpin loop. The existence of a C·U base pair is now proposed, and some additional amino protons are assigned.

Materials and Methods

NMR Samples. Preparation of NMR samples of wheat germ 5S rRNA and its B2 fragment was as described previously (Li et al., 1987), except that the RNA fragments were separated from the digestion mixture by use of Sephadex G-50 (rather than G-75) column chromatography. In addition, the dialysis step was replaced by washing purified RNA (precipitated by ethanol from 10 mM Tris base and 1 M NaCl, pH 7.5) with 75% ethanol twice. The effectiveness of this step for removing buffer components was evidenced by the near absence of a Tris resonance in the proton NMR spectrum. The RNA precipitate was then dissolved in H_2O and lyophilized. The lyophilized RNA was dissolved in a buffer of 10 mM sodium phosphate and 95%/5% H_2O/D_2O, pH 7.0. The final concentration of 5S rRNA was 490 OD (A_{260}) and that of common arm fragment was 168 OD (A_{260}), corresponding to concentrations of about 51 and 17 mg/mL, respectively. In each case, the total sample volume was ~0.4 mL.

One-Dimensional Proton NMR Spectroscopy. All ^1H NMR spectra were obtained with a Bruker AM-500 spectrometer operating at 11.75 T (500 MHz for ^1H). Spectra were recorded at 297 K unless otherwise specified. Chemical shifts are reported in parts per million downfield from 2,2-dimethyl-2-silapentane-5-sulfonate (DSS) as zero, on the basis of an independent calibration. All spectra were subjected to a Lorentz-to-Gauss apodization before Fourier transformation (FT), and no base-line correction was performed. The H_2O

† This work was supported by grants (to A.G.M.) from the U.S. Public Health Service (NIH 1 RO1 GM-29274; NIH 1 S10 RR-01458) and The Ohio State University.

‡ Department of Biochemistry.

§ Department of Chemistry.

0006-2960/90/0429-1722$02.50/0

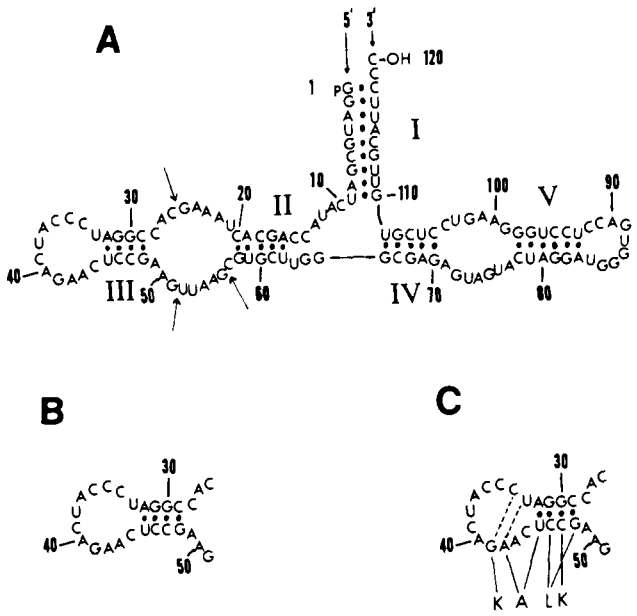

FIGURE 1: Proposed secondary base-pairing schemes for ribosomal 5S rRNA (Luehrsen & Fox, 1981) adapted to the primary nucleotide sequence of intact wheat germ 5S rRNA (A) and one of its enzymatic digestion fragments (B and C). (A) Intact 5S rRNA. Nucleotide residues are numbered from 1 to 120. The five helical regions are labeled I–V. A base pair is denoted by a heavy dot. Arrows denote ribonuclease T1 digestion sites leading to production of the common arm fragment. (B) Common arm (B2) fragment as represented in the Luehrsen–Fox model. (C) Modified common arm base-pairing scheme achieved by addition of the two base pairs shown as dashed lines, with spectral assignments denoted by large letters at bottom right (Li et al., 1987).

peak was suppressed by using a "hard" 1331 pulse sequence (Hore, 1983) with 10-dB transmitter power attenuation (to give a 90° pulse in 44 μs). The Nyquist spectral width was 10638 Hz, and 16K time-domain quadrature data sets were acquired and transformed, resulting in a digital resolution of 1.3 Hz per data point.

The frequency-domain excitation power spectrum of the 1331 pulse was calibrated from a sample of 99.8% D_2O containing a trace of $CuSO_4$ (to reduce the relaxation time of HDO). The transmitter offset was then incremented in 0.5 ppm steps away from the HDO frequency to map out the transmitter power spectrum.

Proton homonuclear NOE experiments were performed as previously described (Chang & Marshall, 1986) with the following modifications. The peak of interest was preirradiated for 0.6 s at a decoupler power of 0.05 mW before data were acquired with the 1331 pulse sequence. Each 16K time-domain data set was Lorentz-to-Gauss apodized and Fourier transformed without subsequent base-line flattening.

Mg^{2+} titration was performed by successive addition of small volumes of 1 M $MgCl_2$ solution to the NMR sample, and spectra were then acquired as described above.

Two-Dimensional Proton NMR Spectroscopy. NOESY spectra in H_2O were recorded in phase-sensitive mode, with pure absorption line shape obtained by use of the time-proportional phase increment (TPPI) method (Redfield & Kunz, 1975; Marion & Wüthrich, 1983). The pulse sequence used was (delay–90°–t_1–90°–t_m–1331–acquire)$_n$. An on-line 4-dB attenuator was used to set the 90° pulse width to 19.7 μs. A total of 4K time-domain data in the t_2 dimension and 174 words in the t_1 dimension were acquired. The delay and the mixing times were both 0.3 s. A total of 1024 scans was accumulated for each t_1 value. The total data acquisition period for the experiment was about 40 h (!). Each time-domain data set was then subjected to a DSA treatment (Haasnoot & Hilbers, 1983), zero-filled to 2K in the t_1 dimension, and Lorentz-to-Gauss apodized in both dimensions before FT. Digital resolution was 5.2 Hz/point in the F_2 dimension and 10.4 Hz/point in the F_1 dimension.

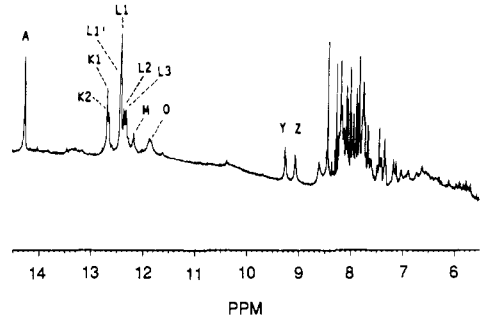

FIGURE 2: Proton 500-MHz NMR spectrum of the B2 fragment, acquired in H_2O at 297 K by use of a 1331 excitation pulse sequence. Downfield resonances are labeled for easy reference.

Table I: Assignments of All Imino and Some Amino Proton Resonances of the Wheat Germ 5S rRNA B2 (Common Arm) Fragment at 297 K

(A) Imino Protons: G–H1 or U–H3

resonance	chemical shift (ppm)	no. of protons	assignment	
A	14.27	2	U_{45} of A_{32}·U_{45}	conformer 1, 2
K1	12.68	1	G_{31} of G_{31}·C_{46}	conformer 1
K2	12.64	1	G_{31} of G_{31}·C_{46}	conformer 2
L1′	12.44	1	G_{30} of G_{30}·C_{47}	conformer 1
L1	12.42	2	U_{33} of C_{44}·U_{33}	conformer 1, 2
L2	12.36	1	G_{30} of G_{30}·C_{47}	conformer 2
L3	12.32	1	G_{48} of G_{48}·C_{29}	conformer 1
M	12.17	1	G_{48} of G_{48}·C_{29}	conformer 2
O	11.84	2	G_{41} or U_{38} (unpaired)	conformer 1, 2

(B) Amino Protons: C–H4(a)/(b) or A–H6(a)/(b)

resonance	chemical shift (ppm)	assignment	
ANH_2(a)/(b)	9.05 (Z)/6.90	A_{32}	conformer 1, 2
$K1NH_2$(a)/(b)	8.43/7.02	C_{46}	conformer 1
$K2NH_2$(a)/(b)	7.91/6.05	C_{46}	conformer 2
$L1'NH_2$(a)/(b)	8.21/6.71	C_{47}	conformer 1
$L1NH_2$(a)/(b)	9.24 (Y)/7.94	C_{44}	?
	8.47/7.48	C_{44}	?
$L2NH_2$(a)/(b)	8.21/6.71	C_{47}	conformer 2

Results and Discussion

Number and Types of Downfield Proton Resonances. In the ^1H NMR spectrum of an RNA in H_2O solution, downfield resonances (i.e., those between 9 and 15 ppm downfield from DSS) arise mainly from imino protons whose chemical shifts quite accurately reflect their *base pair type*: e.g., ~13–15 ppm for A·U and ~11–13 ppm for G·C (Robillard & Reid, 1979). The *number* of downfield resonances for each proton type can then be approximated by spectral integration, provided that one accounts for the nonuniform excitation power as a function of spectral frequency. A 500-MHz ^1H NMR spectrum of the B2 fragment of wheat germ 5S rRNA, including base aromatic, amino, and imino protons, as well as ribose H1′ and 2′-OH protons, is shown in Figure 2. The downfield peaks are labeled alphabetically for easy reference. On the basis of chemical shifts alone, it is clear that only peak A clearly originates from an A·U pair, whereas others originate mainly from G·C pairs. Based on an independent calibration of the 1331 excitation magnitude spectrum (not shown), the number of downfield resonances determined from the B2 spectrum at

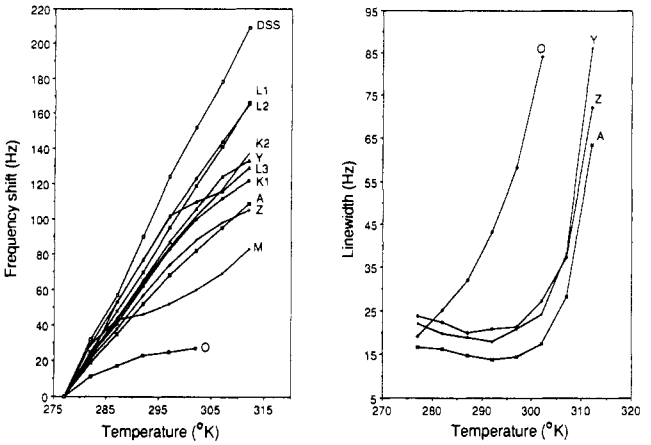

FIGURE 3: Frequency shift (left) and full line width at half-maximum peak height (right) as a function of temperature for downfield 500-MHz ^1H nuclear magnetic resonances from the B2 fragment. For each resonance, the frequency shift at each temperature is reported as its resonant frequency at that temperature minus its resonant frequency at 277 K. The temperature dependence of the chemical shift of the DSS reference was measured independently. Line widths were measured only for the four well-resolved resonances. Data points are simply connected by straight lines.

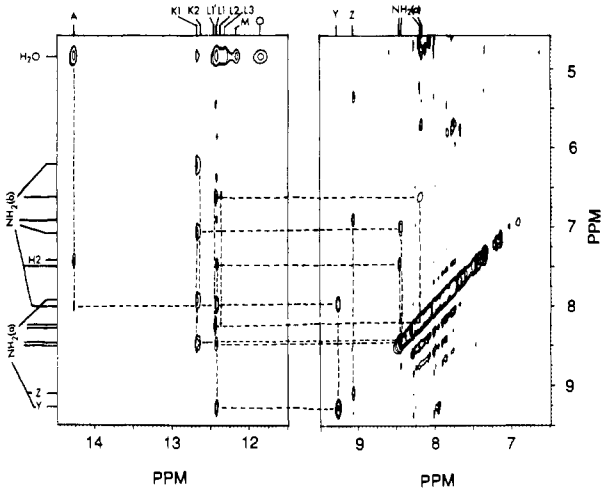

FIGURE 4: Two regions of a phase-sensitive proton homonuclear NOESY spectrum of the B2 fragment at 297 K in H_2O solution. The two expanded regions (F_2 axis: 14.5–11.5 and 9.5–6.5 ppm) were plotted at different contour levels. Cross peaks arising from imino–H_2O, imino–amino (a), imino–amino (b), imino–AH2, and amino(a)–amino(b) are observed. NOE-connected peaks are connected with dashed lines, and downfield peaks are labeled as in Figure 2. See Figure 8 and Table I for assignments.

297 K is shown in Table IA. The presence of at least 10 resonances cannot be accommodated by either the Luehrsen–Fox model (four imino proton base-pair resonances, Figure 1B) or the addition of two extra base pairs to that model (Li et al., 1987; Figure 1C) for the B2 fragment. Even if the Luehrsen–Fox model is assumed to exist in two distinct forms in solution, several downfield resonances must still be explained to account for the observed number of downfield protons.

Temperature Dependence of Downfield Resonances. On increase in temperature, the downfield resonances of 5S rRNA change their chemical shifts and gradually broaden, due to temperature-induced structural changes as well as an acceleration of proton exchange rate with H_2O. The more rapid broadening and smaller temperature-induced chemical shift of the ^1H resonances of helix-terminal and unpaired imino resonances are often used to distinguish them from imino protons in the middle of a base-paired helical segment. Cytosine and adenine *amino* protons may exchange sufficiently slowly with H_2O so as to produce ^1H resonances similar in chemical shift and line width to those of *imino* protons. In contrast, guanine *amino* protons are generally NMR invisible at room temperature, although they may be seen at higher temperatures, as explained by slow rotation of the guanine C2–NH_2 bond (Patel, 1977; McConnell, 1984; Fazakerley et al., 1984) and the "scissor opening" of a G·C pair for solvent access (Fazakerley et al., 1984).

The frequency shift for each resolved proton resonance (relative to *its own* frequency at 277 K) at a series of temperatures from 277 to 317 K is shown in Figure 3 (left). The temperature dependence of the DSS chemical shift is also shown for comparison. Relative to DSS, all resonances shift to higher field upon increase in temperature. The shift could result from weaker H-bonding for that base-pair proton and/or a higher chemical exchange rate between downfield protons and H_2O. The frequency shift vs temperature curves are quite linear for all of the resonances, except for L3, M, and O, which exhibit less temperature-induced shift at high temperature compared to resonances A through L2. The relatively more similar low- and high-temperature environments for resonances L3, M, and O suggest that those resonances likely arise from unpaired imino protons or base-pair protons at the end of a helix. Consistent with this interpretation, we shall later (see below) assign the most "exposed" resonance, peak O, to an unpaired imino proton, and peaks L3 and M to helix-terminal base-pair protons.

In addition, the temperature dependence of the line width at half-maximum peak height for each of the four best-resolved resonances is plotted in Figure 3 (right). The line widths of peaks A, Y, and Z change only slowly from 277 to 302 K and then rapidly increase above that temperature. In contrast, peak O broadens rapidly even at relatively low temperature, again consistent with an unpaired imino proton assignment. Moreover, the intensity of peak O is equivalent to about two protons at 277 K, decreasing to below detectability at or above 307 K.

As seen from Figure 3, the temperature dependences of the frequency shifts and line widths of resonances Y and Z are similar to those of the remaining hydrogen-bonded imino protons. Peaks Y and Z will be assigned to hydrogen-bonded cytidine and adenine amino protons, respectively (see below). Finally, on the basis of the temperature-variation experiments, no guanine amino protons are observed.

Base-Pair Type and Assignment of Some Amino Protons from One-Dimensional and Two-Dimensional NOE Experiments. Proton homonuclear 1-D NOE experiments have been used extensively in both base-pair identification and base-pair sequence determination of 5S rRNAs. The two-dimensional version of the experiment, NOESY, takes longer to perform, but offers several advantages [see, e.g., Wüthrich (1986)]. NOE connectivities between partially overlapped resonances can be observed, and virtually all NOE connectivities can be extracted from a single NOESY experiment. For DNA samples in H_2O solution, NOESY offers a systematic way to assign imino and amino protons (Boelens et al., 1985; Blommers et al., 1987). The extension of the procedure to RNA is straightforward (see below). For the B2 fragment, several structural assignments may be made directly from the single NOESY spectrum shown in Figure 4.

First, for either the cytidine NH_2 of a G·C base pair or the adenine NH_2 of an A·U base pair, the two NH_2 amino protons can be distinguished and assigned. The hydrogen-bonded amino proton NH_2 (a) generally resonates at lower field than the non-hydrogen-bonded proton NH_2 (b) of the same amino

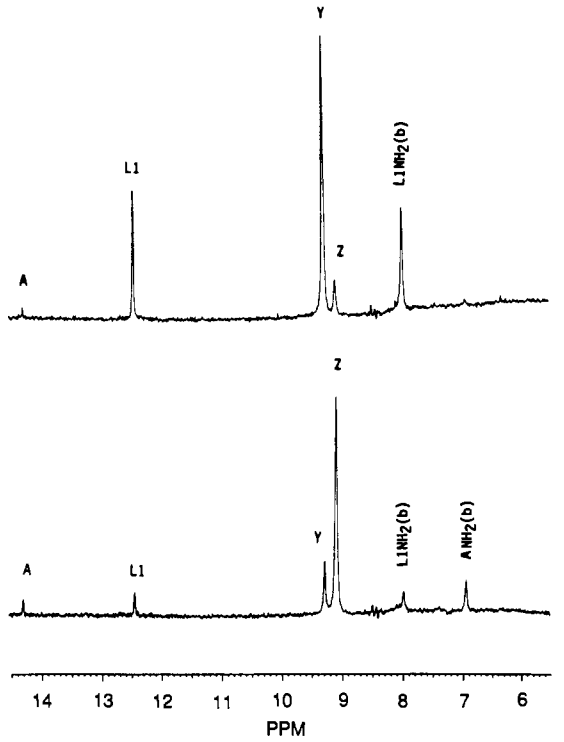

FIGURE 5: 500-MHz proton homonuclear NOE difference spectra for peak Y (top) and peak Z (bottom) from the B2 fragment.

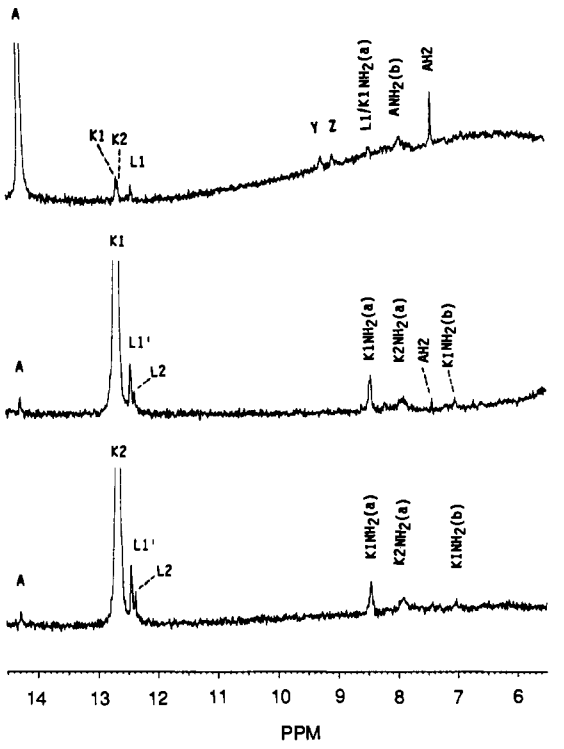

FIGURE 6: 500-MHz proton homonuclear NOE difference spectra for peaks A (top), K1 (middle), and K2 (bottom) from the B2 fragment.

group. Both amino protons are NOE connected to each other as well as to the (same) imino proton of that base pair. Thus, once the imino protons are assigned, the amino protons are assigned automatically (Table IB).

Second, the number of G·C pairs can usually be determined from the number of intra base pair imino–amino cross peaks, because each G·C base pair yields two such cross peaks. Figure 4 clearly shows that resonance L1′ contains one and L1 contains two imino protons: although the two L1 imino protons have the same chemical shift, their amino protons have quite different chemical shifts. The number of imino protons obtained this way is consistent with that inferred from the normal spectrum.

Third, the A·U pair imino–H2 cross peak is observed. For reasons not yet clear, no intra base pair imino–amino cross peaks are visible in Figure 4 for either of the two A·U resonances superimposed as peak A.

Finally, the exchange of imino protons with water can be seen clearly in the uppermost row of cross peaks in Figure 4.

The above-noted assignments of Y and Z as amino protons were confirmed by the 1-D NOE experiments shown in Figure 5. Irradiation at peak Y gave NOE difference peaks at A, L1, and Z and a peak at 7.94 ppm. The prominent NOE difference peaks between Y and L1 and between Y and 7.94 ppm indicate very short Y–L1 and Y–7.94 ppm proton distances, which can be explained only if Y and the 7.94 ppm peak represent amino protons of the same NH_2 group and L1 is the imino proton from the same base pair. Similar reasoning applies to the NOEs between Z and A and between Z and the peak at 6.90 ppm.

As for any molecule of this size, the NOESY results are incomplete and imperfect. For example, imino–imino cross peaks are not observed at all, perhaps because of relatively low RNA concentration. Moreover, peaks K3 and M fail to appear even on the diagonal, although their exchange with H_2O is seen clearly. The proposed two forms of this RNA (see below) cannot be distinguished from NOESY cross peaks involving the two pairs of amino protons NOE connected to resonance L1. Although peak Y contains two amino protons, only one of them can be assigned. Finally, it is not entirely clear why some of the prominent 1-D NOE difference peaks (e.g., between Z and L1 or between Y and Z) are not observed as cross peaks in the corresponding NOESY experiment.

Base-Pair Sequences Inferred from One-Dimensional Imino–Imino NOE Experiments. Because imino–imino cross peaks could not be observed by NOESY of the B2 fragment, 1-D NOE difference experiments were performed for peaks A, K1, and K2 as shown and labeled in Figure 6.

Peak A can be assigned definitely to the only A·U pair (A_{32}·U_{45}) in each form, on the basis of its chemical shift and the appearance of a sharp AH2 NOE difference peak (Figure 6, top). The two resonances of peak A are NOE connected to four other protons: K1, K2, and L1 (two protons). However, in the minimum four base pair model, there is only one base-paired imino proton (G_{31}) next to A_{32}·U_{45}, which should produce only one NOE difference peak on irradiation at peak A. Even if the B2 fragment exists in two distinct conformations, we would expect at most two NOE difference peaks on irradiation at peak A. However (see Figure 1), a uracil (U_{33}) adjoins the A_{32}·U_{45} base pair and could provide an additional NOE difference peak on irradiation at peak A. U_{33} is a particularly good candidate, because the two nucleotides immediately following a helix are usually stacked on the helix (Haasnoot et al., 1986; Blommers et al., 1987).

Upon irradiation of peak A at reduced temperature (277 K, not shown), the NOE difference peak at L1 increased more than that at K1/K2. This result further supports the assignment of L1 as the U_{33} imino proton, which is expected to be more temperature labile than a G·C imino base pair proton. Moreover, the huge Y–L1 and Y–7.94 ppm peak NOEs (Figure 5, top) strongly suggest the formation of a C_{44}·U_{33} pair (Figure 7), in comparison with the T·T pair suggested by NMR in solution (Blommers et al., 1987) and the C·T pair suggested by X-ray diffraction in crystal (Chattopadhyaya et al., 1988). Finally, the very large NOE difference peaks

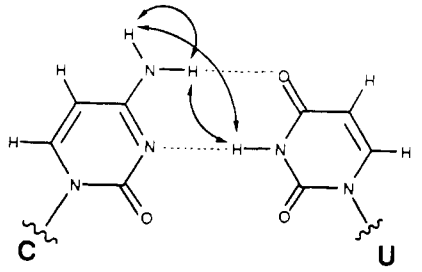

FIGURE 7: Proposed structure for a C·U base pair that may be formed at C_{44}·U_{33}. Hydrogen bonds are shown as dashed lines. The arrows show NOE-detectable short interproton distances within the base pair.

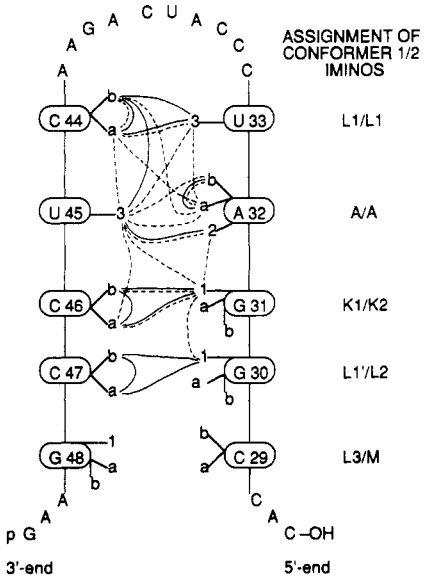

FIGURE 8: Schematic drawing summarizing the observed 1-D (dashed lines) and 2-D (solid lines) NOE connectivities for the wheat germ 5S rRNA B2 fragment in H_2O solution. Proton 1 is GN1, 2 is AH2, 3 is UN3, a is NH2 (a), and b is NH2(b). The assignments of imino protons for the two conformers are listed on the right side of the diagram.

between Y and Z and between Z and L1 (Figure 5) indicate a quite compact and rigid structure around the loop–helix junction, consistent with tight stacking of C_{44}·U_{33} on A_{32}·U_{45}.

The observed NOEs between K1/K2 and L1′ and L2 (Figure 6, middle and bottom) demonstrate that K1/K2 are G_{31} imino protons and that L1′ and L2 are imino protons of G_{30}. Also, the assignment of L1 as a U_{33} imino proton is supported by (a) the absence of K1/K2–L1 NOE; (b) the absence of Y/Z–K1/K2 NOE (but a large Y/Z–L1 NOE); and (c) the presence of an NOE difference peak at A on irradiation at Y, Z, or K1/K2.

Resonances L3 and M are assigned to G_{48} imino protons due to their relatively fast exchange with H_2O protons as shown by heat-induced melting experiments. Peak O, which melts at a very low temperature, shows no NOE connectivity (not shown) to any other peak. Thus, it may be assigned to an imino proton from either U_{38} or G_{41} in the hairpin loop (Haasnoot et al., 1980). The single-stranded terminal imino proton of G_{51} is not likely to be observable, as noted previously (Li et al., 1987). For ease in reference, the observed NOE connectivities in 1-D and 2-D experiments described to this stage are summarized in Figure 8, and the assignments of imino and amino protons are listed in Table I. Spin diffusion is not important in these measurements, since a reduction in preirradiation period from 0.6 to 0.3 s gave qualitatively similar results (not shown) for peak A.

Assignment of ^1H NMR Resonances to Each of Two Forms

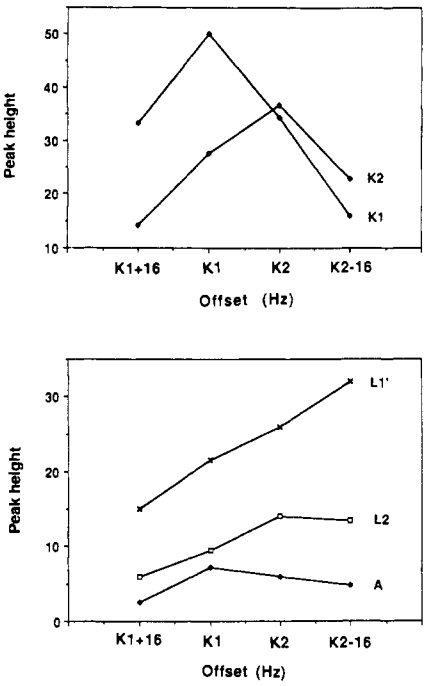

FIGURE 9: (Top) 500-MHz proton 1-D NOE difference spectral peak heights (arbitrary scale) for two partially overlapped resonances, K1 and K2, as a function of irradiation frequency varied in increments of 16 Hz (i.e., the difference between the K1 and K2 resonance frequencies) for the B2 fragment. The abscissa denotes the frequency of on-resonance irradiation. The off-resonance irradiation frequency (5970 Hz downfield from the carrier frequency) was the same in all four cases. (Bottom) Peak heights for three other resonances that are NOE-connected to K1 and K2 (see Figure 6). Scaling is as in the top diagram, except that these NOE difference peaks are smaller by about 13–14 times than those in the top diagram.

of the B2 Fragment. As noted above, two stable conformers of the B2 fragment are necessary to account for the observed number of resonances and NOE connectivities. In particular, K1 and K2 are both G·C imino protons, but both are spatially adjacent to the same (unique) A·U base pair. Thus, K1 and K2 must be the same G_{31} imino proton in two conformers. Irradiation at K1 and K2 should therefore serve to (a) identify the other base pair immediately adjacent to K1 and K2 (see above) and (b) test whether or not the two forms of B2 interconvert with a lifetime faster than T_1 (~0.1–0.4 s). [We already know that the two forms do not interconvert faster than their resolved chemical shift difference, $1/\tau_{ex} < 2\pi(16\ \text{Hz}) \cong 100\ \text{s}^{-1}$.] Because K1 and K2 nearly overlap (16-Hz peak separation), it is not possible to irradiate one resonance without power spillover to the other resonance in a 1-D experiment. Therefore, NOE difference experiments were also conducted by irradiation either at 16 Hz downfield of K1 or at 16 Hz upfield of K2. The difference spectral peak heights of resonances K1 and K2 and the heights of resonances A, L1′, and L2 in those experiments are shown in Figure 9.

Figure 9 shows that the NOE connectivity to peak A is maximal on irradiation at peak K1, whereas NOE connectivity to peak L2 is maximized by irradiation at K2. We may therefore tentatively assign imino proton resonances L1–A–K1–L1′ to one form (henceforth denoted conformer 1) and imino proton resonances L1–A–K2–L2 to another (conformer 2). The reason the NOE difference peak height for L1′ increases continuously as the irradiation frequency decreases is not yet clear.

Additional assignments may be inferred from the relative populations of the two forms, as reflected by the ratio between corresponding peak heights in the two forms. As seen in Figure

2, the ratios for K1 to K2, L1′ to L2, and L3 to M are nearly the same, namely, ~3:2. In fact, populations inferred from the normal proton spectrum are more reliable than those based upon NOEs, due to the poorer signal-to-noise ratio and irradiation offset effects in NOE experiments. Summarizing to this point, we assign B2 fragment imino proton resonances to conformer 1, L1–A–K1–L1′–L3, and conformer 2, L1–A–K2–L2–M (see also Figure 8).

The Two Forms Are Interconvertible. Magnetization transfer can occur by means of intramolecular dipolar coupling as well as by means of chemical exchange (in this case, interconversion of conformers). Thus, if we can detect magnetization transfer between resonances K1 and K2, which are assigned to the same proton in the two different conformers, we will establish that interconversion occurs with an inverse lifetime faster than $1/T_1 \cong 5–20\ s^{-1}$. Two slowly interconverting conformers of *Escherichia coli* $tRNA^{phe}$ at low Mg^{2+} concentrations have been identified this way (Hyde & Reid, 1985). From Figure 9 (top), it is clear that magnetization transfer between K1 and K2 indeed takes place, because the NOE difference peak height for K1 (or K2) is greater (by 3% and 17%, respectively) on irradiation at K2 (or K1) than at the same offset on the opposite side of K1 (or K2). The large magnitude of the effect further confirms that the magnetization transfer occurs via chemical exchange, since imino–imino dipolar couplings typically produce NOE difference peaks less than 5% of the original peak height. Finally, the observed asymmetry in magnetization-transfer magnitude may reflect different intrinsic T_1s for the same imino proton (K1 and K2) in the two forms, as previously observed and explained in the case of *E. coli* $tRNA^{phe}$ (Hyde & Reid, 1985).

As for assignment of NOE connectivities, discrimination between dipolar and chemical exchange effects for partially overlapped resonances is in principle better achieved by means of NOESY rather than 1-D NOE measurements. Unfortunately, NOESY was not practical in this case, because of the need for too-high RNA concentration (at which aggregation would vitiate interpretation) and limited spectral resolution (so that K1–K2 cross peaks could overlap with diagonal peaks).

Two Conformers Are Still Present in Solutions Containing Mg^{2+}. It has long been known that Mg^{2+} can stabilize 5S rRNA molecules and induce structural changes. On titration of the downfield ^1H NMR resonances of 5S rRNA (or its fragments) with Mg^{2+}, the following changes have been observed: (a) increase in total spectral area, indicating an increase in total number of base pairs; (b) increase in the melting temperature, indicating an increase in RNA stability; and (c) shift in resonance frequency. Although Mg^{2+} titrations have been performed on *E. coli* 5S rRNA and its fragments (Leontis et al., 1985; Leontis & Moore, 1986b), the Mg^{2+}-induced structural changes have not yet been fully characterized. Moreover, due to limited spectral resolution in prior Mg^{2+} titration of the B2 fragment of wheat germ 5S rRNA, accurate spectral changes could not be determined (Li et al., 1987). That experiment was therefore repeated, and the results are shown in Figure 10.

All of the downfield resonances are still observed on addition of Mg^{2+}, and no new resonances appear. The relative peak areas (i.e., the relative populations) of resonances from the two conformers are also unchanged. All of the resonances shift to lower field, indicating stronger H-bonding and/or a tighter helix twist. This Mg^{2+}-binding effect is further supported by ^{31}P NMR results (Wu & Marshall, 1990).

The frequency shift for each resonance (relative to *its own* resonance frequency in the absence of Mg^{2+}) is plotted in

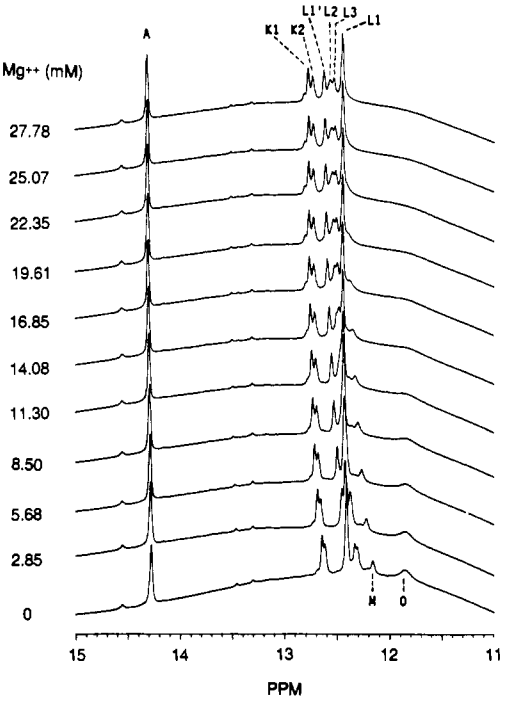

FIGURE 10: Mg^{2+} titration of the 500-MHz proton downfield spectrum of the B2 fragment. Resonances are better resolved in the presence of Mg^{2+} and are labeled as in Figure 2.

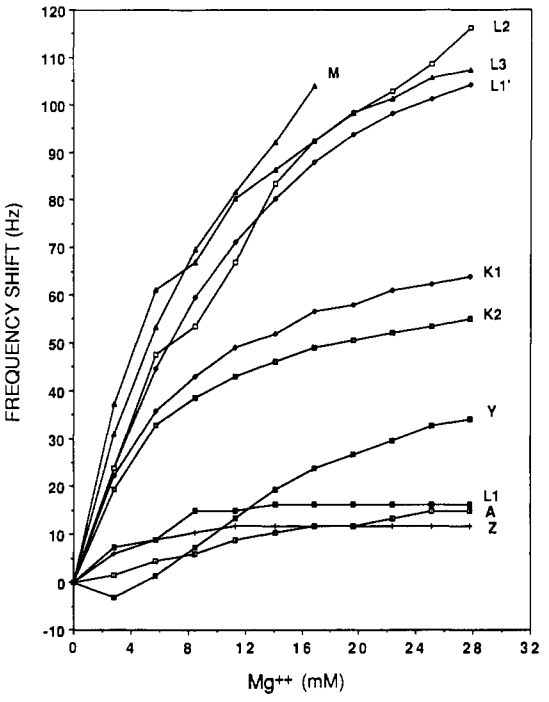

FIGURE 11: Mg^{2+}-induced frequency shifts for the downfield 500-MHz ^1H resonances of the B2 fragment. For each resonance, the shift at a given Mg^{2+} concentration represents the difference between the resonant frequency at that Mg^{2+} concentration and the resonant frequency of the same peak in the absence of Mg^{2+}. Data points are simply connected by straight lines.

Figure 11. Note that the shift magnitudes for each of the two resonances assigned to the same proton in the two conformers are similar, and that the shift magnitude gradually increases from loop side to the open side of the helix (bottom to top in Figure 11). This behavior further supports our prior interpretation, since the Mg^{2+}-induced helix twisting is more pronounced for base pairs on the open side of the helix than on the loop side. There is no apparent Mg^{2+}-induced change

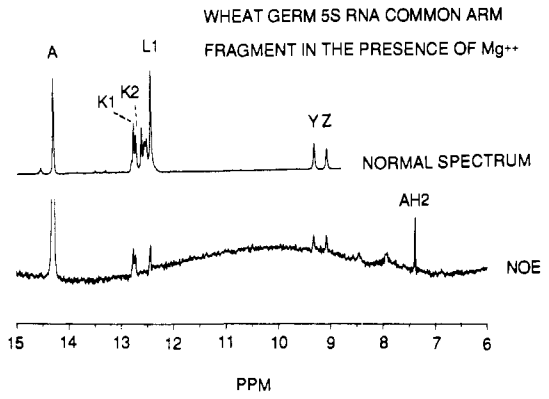

FIGURE 12: (Top) Normal 500-MHz ^{1}H NMR spectrum (i.e., a base-line-flattened plot of the data from the uppermost spectrum in Figure 10). (Bottom) 500-MHz ^{1}H 1-D NOE difference spectrum for resonance A of the B2 fragment in the presence of 27.78 mM Mg^{2+}.

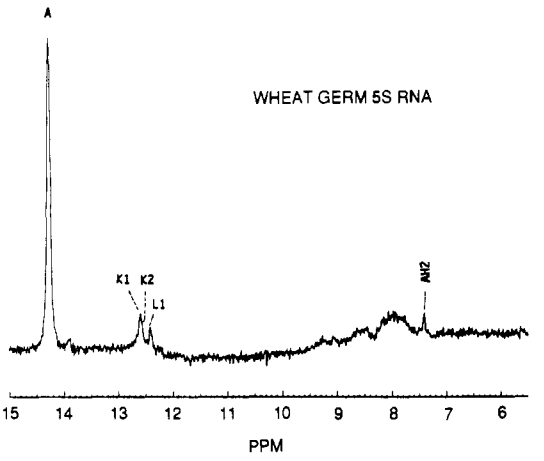

FIGURE 13: 500-MHz proton homonuclear NOE difference spectrum for resonance A in intact wheat germ 5S rRNA.

in line width for any resonance, except that resonance O gradually broadens and finally cannot be seen above 20 mM Mg^{2+}. The broadening of peak O may reflect the opening of that part of the loop, such that H_2O is more accessible to resonance O in the presence of Mg^{2+}.

1-D NOE experiments on peaks A, Y, and Z were performed after the final incremental addition of Mg^{2+}. The same NOE connectivities were found as in the absence of Mg^{2+}. The result of irradiation of peak A is shown in Figure 12, which clearly shows the A–L1 NOE connectivity but none from A to L1′ (since resonances L1′ and L1 can now be resolved). This result therefore not only serves to confirm the resonance assignments obtained in the absence of Mg^{2+} but also shows that addition of Mg^{2+} does not change the base-pairing pattern of the B2 fragment.

Structural Differences between the Two 5S rRNA Conformers. We can make some limited structural inferences about the B2 fragment from the above ^{1}H NMR experiments in H_2O solution. First, the two conformers differ in the degree of the H-bonding in the helical base-paired segment (i.e., one conformer can be regarded as having a more "open" helix than the other), since each base-paired imino proton resonance of conformer 1 is shifted further downfield than its counterpart in conformer 2 (see Figure 2), suggesting stronger H-bonding (or tighter helix structure) for conformer 1. Second, chemical shift differences between corresponding resonances in the two forms increase on proceeding from the loop end of the helix to the open end: peaks L1 (two protons) and A (two protons) show no chemical shift difference between the two RNA forms; peaks K1 and K2 differ by 16 Hz; peaks L1′ and L2 differ by 39 Hz; and peaks L3 and M differ by 64 Hz. In other words, the two forms differ more and more as one proceeds toward the open end of the helical stem. Finally, only *one* adenine H2 NOE difference peak was seen on irradiation at peak A (A·U pair), indicating very similar environments for the A·U pair in the two forms. 1-D and 2-D NMR experiments performed for the B2 fragment in D_2O solution further corroborate these conclusions (Wu & Marshall, 1990).

The Common Arm Fragment Has Two Conformations in Intact Wheat Germ 5S rRNA. In view of the potential structure-altering effects of enzymatic cleavage and preparative manipulations, it is important to establish whether the two forms detected here occur only in the isolated B2 fragment or are present in native wheat germ 5S rRNA. Therefore, the 1-D NOE difference spectrum produced by irradiation at peak A was repeated on intact wheat germ 5S rRNA (Figure 13). Peak A showed the same NOE connectivities as in the B2 fragment (Figure 6, top). Since peak A arises only from the B2 fragment (Li et al., 1987), it is clear that the intact wheat germ 5S rRNA also exhibits two B2 conformations. However, the present data do not allow us to say whether the two conformations in intact 5S rRNA interconvert as they do in the isolated B2 fragment.

Comparison of the spectra in Figures 6 (top) and 13 shows that on proceeding from the B2 fragment to intact 5S rRNA peaks K1 and K2 shift upfield by ~0.1 ppm, whereas peaks A, L1, and adenine H2 do not shift. We conclude that (a) the B2 helix is less flexible on the loop end than on the open end and (b) that the B2 helix is affected (but not greatly) by the presence of the other parts of the intact 5S rRNA molecule.

Comparison to Prior Work and Implications of the Present Results. Compared to the recent prior study of the B2 fragment (Li et al., 1987), we have made three experimental improvements: (a) use of Sephadex G-50 rather than G-75 in fragment separation to produce a purer sample; (b) increased time-domain data size to 16K (rather than 4K) in all 1-D experiments to provide higher digital resolution and thus a more accurate definition of resonance line shape; and (c) assignments based on additional 2-D NOE experiments in H_2O solution. As a result, we have been able to resolve and assign more resonances. In addition, our reported spectral magnitudes have been corrected for variation of excitation power with frequency. For the 1-D NOE difference experiments, the increased digital resolution brings dramatic improvements: in addition to previously observed imino–*imino* ^{1}H NOE difference peaks, imino–*amino* proton NOE peaks were also observed in 5S rRNA for the first time. Moreover, in each case, the imino–amino proton NOEs are consistent with those obtained from the NOESY experiment. Interestingly, imino–amino cross peaks are observed for 4K data sets in the NOESY experiment but not in its 1-D equivalent, presumably because of the difference-spectrum nature of the latter. Finally, the 4-fold improved digital resolution has helped us to clarify some of the ambiguities between imino–imino proton NOEs: e.g., from resonance A to resonances K1 *and* K2 instead of simply resonance A to (unresolved) resonance K.

Although none of the experimental results in our prior paper (Li et al., 1987) is wrong, the above improvements have allowed us to recognize the presence of two conformational forms of wheat germ 5S rRNA (native or the B2 fragment). The two conformers are in mutual slow exchange (with respect to their chemical shift differences), with an equilibrium ratio (K1:K2) of ~3:2 (Figure 2), reflecting the relative lifetimes of the two conformers (Hyde & Reid, 1985).

The two forms are definitely not the same as the well-known A and B conformers in *E. coli* 5S rRNA, in which the B form is denatured (Aubert et al., 1968; Richards et al., 1973; Weidner et al., 1977; Weidner & Crothers, 1977; Noller & Garrett, 1979; Jagadeeswaran & Gherayil, 1980; Burns et al., 1980). Neither are they the dynamic conformers generated by "bulge migration" (De Wachter et al., 1982, 1984), because the two conformers have the *same* base pair sequence. Moreover, the bulge migration mechanism is not expected to operate in this small fragment with such a short helical segment. Because no dimer is formed in the present experiments, the two conformers are not monomer and dimer, as discussed earlier (Li et al., 1987).

The two forms seen here are not different RNase T1 digestion fragments and are therefore not related to the *E. coli* 5S rRNA A_L and A_H forms found by temperature-jump experiments (Kao & Crothers, 1980; Rabin et al., 1983; Christensen et al., 1985), of which the two forms exchange by means of a proton-coupled conformational switch. Two conformations of *E. coli* 5S rRNA proposed on the basis of Mg^{2+}-induced NMR spectral changes of nonexchangeable protons (Kime & Moore, 1982) were shown to be different from the A_L and A_H forms (Leontis et al., 1985; Leontis & Moore, 1986b). Although different structures have been observed in *E. coli* 5S rRNA helices II and III upon heating (Leontis & Moore, 1986a), the spectral changes induced by Mg^{2+} addition (or heating) were smooth and continuous and gave no means for clear distinction between two (or more) conformations. Finally, we cannot say whether or not the two conformers seen here are related to the A and A′ forms of rat liver 5S rRNA (Muller et al., 1985) determined by X-ray scattering and circular dichroism.

All of the above conformational changes were induced by subjecting the RNA to different conditions (e.g., temperature, salt concentration). In contrast, the two conformers observed in the present experiments represent a true equilibrium between two stable structures. In this respect, the two B2 conformers reported here are very like these found in $tRNA^{phe}$ (Hyde & Reid, 1985).

Putative biological functions for two interconvertible forms of 5S rRNA (e.g., as a conformational switch in protein biosynthesis) have been repeatedly offered [e.g., Weidner et al. (1977), Jagadeeswaran and Cherayil (1979), and Christensen et al. (1985)], but so far without firm experimental evidence. The possible biological function of the two conformers here is not clear. On the basis of results from D_2O solution (Wu & Marshall, 1990), we do not anticipate their role in this kind of conformational switch, because the conformational change is probably too small.

Finally, our presently proposed common arm structures no longer allow base pairing in the hairpin loop [in contrast to Li et al. (1987)]. However, base *stacking* (as opposed to intraloop base *pairing*) may possibly extend into the hairpin loop (Wu & Marshall, 1990) and could also account for the observed lack of binding between the highly conserved single-stranded GTψC segment of tRNA and the Watson–Crick complementary conserved GAAC segment of the 5S rRNA common arm.

Acknowledgments

We thank E. S. Maxwell at North Carolina State University for his generous assistance in training one of us (J.W.) to perform RNA sequencing of the B2 fragment in his laboratory. We also thank C. E. Cottrell for his advice in setting up the NMR experiments, and S.-J. Li for valuable discussions and assistance. The generous donation of wheat germ by International Multifoods (Columbus, OH) is much appreciated.

Registry No. C, 71-30-7; U, 66-22-8; Mg, 7439-95-4.

References

Aubert, M., Scott, J. F., Reynier, M., & Monier, R. (1968) *Proc. Natl. Acad. Sci. U.S.A. 61*, 292–299.

Blommers, M. J. J., Haasnoot, C. A. G., Hilbers, C. W., Van Boom, J. H., & Van der Marel, G. A. (1987) in *Structure and Dynamics of Biopolymers* (Nicolini, C., Ed.) pp 78–91, Martinus Nijhoff Publishers, Dordrecht, The Netherlands.

Boelens, R., Scheek, R. M., Dijkstra, K., & Kaptein, R. (1985) *J. Magn. Reson. 62*, 378–386.

Burns, P. D., Luoma, G. A., & Marshall, A. G. (1980) *Biochem. Res. Commun. 96*, 805–811.

Chang, L.-H., & Marshall, A. G. (1986) *Biochemistry 25*, 3056–3063.

Chattopadhyaya, R., Ikuta, S., Grzeskowiak, K., & Dickerson, R. E. (1988) *Nature (London) 334*, 175–179.

Christensen, A., Mathiesen, M., Peattie, D., & Garrett, R. (1985) *Biochemistry 24*, 2284–2291.

Delihas, N., & Andersen, J. (1982) *Nucleic Acids Res. 10*, 7323–7344.

Delihas, N., & Andersen, J. (1984) *Prog. Nucleic Acid Res. Mol. Biol. 31*, 161–190.

De Wachter, R., Chen, M.-W., & Vandenberghe, A. (1982) *Biochimie 64*, 311–329.

De Wachter, R., Chen, M.-W., & Vandenberghe, A. (1984) *Eur. J. Biochem. 143*, 175–182.

Fazakerley, G. V., Van der Marel, G. A., Van Boom, J. H., & Guschlbauer, W. (1984) *Nucleic Acids Res. 12*, 8269–8279.

Fox, G. E., & Woese, C. R. (1975) *Nature (London) 256*, 505–507.

Haasnoot, C. A. G., & Hilbers, C. W. (1983) *Biopolymers 22*, 1259–1266.

Haasnoot, C. A. G., Den Hartoy, J. H. J., De Tooy, F. M., Van Boom, J. H., & Altona, C. (1980) *Nucleic Acids Res. 8*, 169–181.

Haasnoot, C. A. G., Hilbers, C. W., Van der Marel, G. A., Van Boom, J. H., Singh, U. C., Pattabiraman, N., & Kollman, P. A. (1986) in *Biomolecular Stereodynamics IV*, Proceedings of the Fourth Conversation in the Discipline Biomolecular Stereodynamics, SUNY at Albany, NY, June 4–9, 1985 (Sarma, R. H., & Sarma, M. H., Eds.) pp 101–115, Adenine Press, New York.

Hare, D. R., & Reid, B. R. (1982a) *Biochemistry 21*, 1835–1842.

Hare, D. R., & Reid, B. R. (1982b) *Biochemistry 21*, 5129–5135.

Hore, P. J. (1983) *J. Magn. Reson. 54*, 539–542.

Hyde, E. I., & Reid, B. R. (1985) *Biochemistry 24*, 4315–4325.

Jagadeeswaran, P., & Cherayil, J. D. (1980) *J. Theor. Biol. 83*, 369–375.

Johnston, P. D., & Redfield, A. G. (1978) *Nucleic Acids Res. 5*, 3913–3927.

Johnston, P. D., & Redfield, A. G. (1981) *Biochemistry 20*, 1147–1156.

Kao, T. H., & Crothers, D. M. (1980) *Proc. Natl. Acad. Sci. U.S.A. 77*, 3360–3364.

Kime, M. J., & Moore, P. B. (1982) *Nucleic Acids Res. 10*, 4973–4983.

Leontis, N. B., Ghosh, P., & Moore, P. B. (1985) in *Biomolecular Stereodynamics IV*, Proceedings of the Fourth Conversation in the Discipline Biomolecular Stereodynamics, SUNY at Albany, NY, June 4–9, 1985 (Sarma, R. H.,

& Sarma, M. H., Eds.) pp 287-306, Adenine Press, New York.
Leontis, N. B., Ghosh, P., & Moore, P. B. (1986a) *Biochemistry 25*, 3916-3925.
Leontis, N. B., Ghosh, P., & Moore, P. B. (1986b) *Biochemistry 25*, 7386-7392.
Li, S.-J., & Marshall, A. G. (1985) *Biochemistry 24*, 4047-4052.
Li, S.-J., & Marshall, A. G. (1986) *Biochemistry 25*, 3673-3682.
Li, S.-J., Wu, J., & Marshall, A. G. (1987) *Biochemistry 26*, 1578-1585.
Luehrsen, K. R., & Fox, G. E. (1981) *Proc. Natl. Acad. Sci. U.S.A. 78*, 2150-2154.
Marion, D., & Wüthrich, K. (1983) *Biochem. Biophys. Res. Commun. 113*, 967-974.
Marshall, A. G., & Wu, J. (1990) *Biol. Magn. Reson. 9*, 55-118.
McConnell, B. (1984) *J. Biomol. Struct. Dyn. 1*, 1407-1421.
Muller, J. J., Misselwitz, R., Zirwer, D., Damaschun, G., & Welfle, H. (1985) *Eur. J. Biochem. 148*, 89-95.
Nishikawa, K., & Takemura, S. (1974) *J. Biochem. (Tokyo) 76*, 935-947.
Noller, H. F., & Garrett, R. A. (1979) *J. Mol. Biol. 132*, 621-636.
Patel, D. J. (1977) *Biopolymers 16*, 1635-1656.
Rabin, D., Kao, T. H., & Crothers, D. M. (1983) *J. Biol. Chem. 258*, 10813-10816.
Redfield, A. G., & Kunz, S. D. (1975) *J. Magn. Reson. 19*, 250-254.
Richard, E. G., Lecanidou, R., & Geroch, M. E. (1973) *Eur. J. Biochem. 34*, 262-267.
Robillard, G. T., & Reid, B. R. (1979) in *Biological Applications of Magnetic Resonances* (Shulman, R. G., Ed.) pp 45-112, Academic Press, New York.
Roy, S., Papastavros, M. Z., & Redfield, A. G. (1982) *Biochemistry 21*, 6081-6088.
Sanchez, V., Redfield, A. G., Johnston, P. D., & Tropp, J. (1980) *Proc. Natl. Acad. Sci. U.S.A. 77*, 5659-5662.
Weidner, H., & Crothers, D. M. (1977) *Nucleic Acids Res. 4*, 3401-3414.
Weidner, H., Yuan, R., & Crothers, D. M. (1977) *Nature (London) 266*, 193-194.
Wolters, J., & Erdmann, V. A. (1988) *Nucleic Acids Res. 16*, r1-r45.
Wu, J., & Marshall, A. G. (1990) *Biochemistry* (following paper in this issue).
Wüthrich, K. (1986) *NMR of Proteins and Nucleic Acids*, Wiley, New York.

Wheat Germ 5S Ribosomal RNA Common Arm Fragment Conformations Observed by ^1H and ^{31}P Nuclear Magnetic Resonance Spectroscopy†

Jiejun Wu‡ and Alan G. Marshall*,‡,§
Department of Biochemistry, 484 West 12th Avenue, and Department of Chemistry, 120 West 18th Avenue, The Ohio State University, Columbus, Ohio 43210
Received July 31, 1989

ABSTRACT: The *nonexchangeable* protons of the common arm fragment of wheat germ (*Triticum aestivum*) ribosomal 5S RNA have been observed by means of high-resolution 500-MHz ^1H NMR spectroscopy in D_2O solution. Although NMR studies on the *exchangeable* protons support the presence of two distinct solution structures of the common arm fragment (and of the same base-paired segment in intact 5S rRNA), only a single conformation is manifested in the ^1H NMR behavior of all of the H6 and H5 pyrimidine and most of the H8/H2 purine protons under the same salt conditions. The nonexchangeable protons near the base-paired helix have been assigned by a sequential strategy. Conformational features such as the presence of a cytidine–uridine (C·U) pair at the loop–helix junction and base stacking into the hairpin loop are evaluated from nuclear Overhauser enhancement spectroscopy (NOESY) data. Double-quantum filtered correlation spectroscopy (DQF-COSY) experiments show that most of the 26 riboses are in the C3′-endo conformation. Finally, backbone conformational changes induced by Mg^{2+} and heating have been monitored by ^{31}P NMR spectroscopy. Our results show that the common arm RNA segment can assume two conformations which produce distinguishably different NMR environments at the base-pair hydrogen-bond imino protons but not at nonexchangeable base or ribose proton or backbone phosphate sites.

Recent developments in NMR methodology (in conjunction with large-scale synthesis of oligonucleotides of defined sequences) have produced much recent progress in knowledge in nucleic acid solution structure and dynamics [for reviews, see Gronenborn and Clore (1985), Patel et al. (1987), Hosur et al. (1988), and Van de Ven & Hilbers (1988)]. For example, general resonance assignment procedures have been applied for double-stranded synthetic RNA oligomers which generally form A-type helices. Detailed structural information for smaller oligomers (say, <10000 Da) may be obtained from analysis of ^1H–^1H and/or ^1H–^{31}P coupling constants, ^1H–^1H dipolar cross-relaxation data, extensive computer modeling, or a combination of the above (Clore et al., 1985; Lankhorst et al., 1985; Happ et al., 1988; Van den Hoogen et al., 1988; Chou et al., 1989).

For nucleic acids of larger size (>10000 Da), NMR studies are usually limited to the downfield exchangeable proton region (9–15 ppm from DSS) or to nuclei other than protons (^{31}P, ^{13}C, ^{15}N), due to extensive ^1H NMR peak overlap. For ex-

† This work was supported by grants (to A.G.M.) from the U.S. Public Health Service (NIH 1 R01 GM-29274; NIH 1 S10 RR-01458) and The Ohio State University.
‡ Department of Biochemistry.
§ Department of Chemistry.

0006-2960/90/0429-1730$02.50/0